Circinis X-1 revisited: fast-timing properties in relatio to spectral state

Oosterbroek, T.; van der Klis, M.; Kuulkers, E.; van Paradijs, J.A.; Lewin, W.H.G.

Publication date
1995

Published in
Astronomy & Astrophysics

Astron. Astrophys. 297, 141–158 (1995)

ASTRONOMY
AND
ASTROPHYSICS

Circinus X-1 revisited: fast-timing properties in relation to spectral state

T. Oosterbroek[1], M. van der Klis[1], E. Kuulkers[1], J. van Paradijs[1], and W.H.G. Lewin[2]

[1] Astronomical Institute "Anton Pannekoek", University of Amsterdam, and Center for High Energy Astrophysics, Kruislaan 403, NL-1098 SJ Amsterdam

[2] Massachusetts Institute of Technology, 37-627, Cambridge, MA 02139, USA

Received 8 September 1994 / Accepted 18 October 1994

Abstract. We have studied the X-ray spectral and fast-timing variations of Cir X-1 by performing a homogenous analysis of all *EXOSAT* ME data on this source using X-ray hardness-intensity diagrams (HIDs), colour-colour diagrams (CDs), and power spectra. Cir X-1 exhibits a wide range of power spectral shapes and a large variety in X-ray spectral shapes. At different epochs the power spectra variously resemble those of an atoll source, a Z source, a black-hole candidate, or are unlike any of these. At some epochs one-dimensional connected-branch patterns are seen in HID and CD, and at other times more complex structures are found. We interpret the complex behaviour of Cir X-1 in terms of a model where accretion rate, orbital phase and epoch are the main determinants of the source behaviour, and where the unique properties of the source are due to two special circumstances: (i) the source is the only known atoll source (accreting neutron star with a very low magnetic field) that can reach the Eddington critical accretion rate, and (ii) it has a unique, highly eccentric and probably precessing orbit. Property (i) makes Cir X-1 a very important source for our understanding of the similarities in the observable properties of neutron stars and black holes as it allows to separate out black hole signatures from properties that are merely due to the presence of an accreting compact object with a low magnetic field.

Key words: accretion, accretion disks – X-rays: stars – individual: Cir X-1 – binaries: close

1. Introduction

Cir X-1 is one of the most puzzling X-ray binaries. It was first detected in X-rays by Margon et al. (1971), who in the discovery observation found evidence for pulsations at a frequency of 1.4 Hz (see also Sect. 4.3). At times Cir X-1 is one of the brightest sources in the X-ray sky (~10 c/s/cm^2 in the 1-20 keV band), while at other times it is very weak (~0.01 c/s/cm^2). The source shows periodic radio flares which suggest an orbital period of 16.6 days (Nicolson 1980; for a recent ephemeris see Stewart et al. 1991), and possibly emits radio jets (Stewart et al. 1993). The radio flares are accompanied by abrupt changes in the X-ray light curve (Kaluzienski et al. 1976). During the early 1970's Cir X-1 tended to be in a high state during most of its 16.6 day cycle (Jones et al. 1974), while in the mid-seventies it was in a low state during the largest part of its cycle (Kaluzienski et al. 1976). Murdin et al. (1980) proposed that an eccentric high-mass binary model for Cir X-1 could explain this evolution of the light curve on a time scale of a few years. The optical counterpart of Cir X-1 is a faint red star (Moneti 1992). The high L_X/L_{opt} indicates that Cir X-1 is a low-mass X-ray binary (LMXB).

At one time, the compact object in Cir X-1 was suspected to be a black hole on the basis of rapid variability similar to that observed in Cyg X-1 (Toor 1977). However, the presence of a low magnetic field neutron star in the system was demonstrated by the detection of type I X-ray bursts (Tennant et al. 1986a,b). The source shows quasi periodic oscillations (QPO) in the range 6–20 Hz (Tennant 1987,1988b; Makino et al. 1992) and 1.4 Hz (Tennant 1988a), which in this frequency range are also observed in other low magnetic field compact objects (neutron stars as well as black holes; see van der Klis 1994a for a recent review).

The study of the X-ray spectral and fast-timing properties of accreting low magnetic field neutron stars has led to a division into two groups: the so-called Z sources and atoll sources (Hasinger & van der Klis 1989, hereafter HK89; for reviews see van der Klis 1989a, 1991). As we shall see, Cir X-1 exhibits some properties of sources in both groups as well as of black hole candidates. For that reason, we here briefly summarize the properties of these sources to the extent relevant to a comparison with Cir X-1.

Send offprint requests to: T. Oosterbroek

1.1. Z and atoll sources

The Z sources tend to be more luminous than the atoll sources and have a Z-shaped track (i.e. 3 distinct branches) in the X-ray colour-colour diagram (CD). Z sources show two different kinds of QPO. In the topmost stroke of the Z, the *horizontal branch*, where $\dot{M}$ is thought to be lowest, QPO with a frequency of 13-55 Hz are present; in the middle stroke, the *normal branch* (or a part of it) QPO are found with a lower frequency (5–7 Hz), which is approximately the same in all Z sources. When the sources move into the bottom stroke of the Z, the *flaring branch*, this frequency increases to 20 Hz (in Sco X-1 and GX 17+2, Dieters & van der Klis 1995; Penninx et al. 1990). Atoll sources show neither of these two types of QPO.

Z and atoll sources show two types of broad noise components in their power spectra: power-law noise and band-limited noise. Both Z and atoll sources show a power-law noise component called *very low frequency noise*. It dominates the power spectrum below ~ 0.01 Hz and has a power-law shape $P \propto \nu^{-\alpha}$ with an index $\alpha \sim 1.5$ in atoll sources, and ~ 1.5–2 in Z sources. Z sources show, in addition to the very low frequency noise, two types of band limited noise. One, the *low-frequency noise* is present only at low $\dot{M}$, when horizontal branch QPO are present; this component has an exponentially cut-off power law shape with a cut-off of typically 2-20 Hz. The other, *high frequency noise* is always present. The cut-off frequency of this component is 50–100 Hz. Atoll sources show only one type of band limited noise. It is present at low $\dot{M}$, in the so-called *island state*, and disappears at higher $\dot{M}$, in the so-called *banana state* (HK89). This component has cut-off frequencies of 0.3–20 Hz, and is, confusingly, also called high-frequency noise. Van der Klis (1994b) suggested that the *low* frequency noise in Z sources is similar to the so-called *high* frequency noise in atoll sources (the two noise types have similar cut-off frequencies and similar dependencies on mass accretion rate), whereas the high frequency noise in Z sources is a different component.

The physical distinction between Z and atoll sources is thought to be the strength of the magnetic field of the neutron star. Z sources are thought to have a relatively high ($\sim 10^9$ Gauss) magnetic field, while the field of the atoll sources is thought to be weaker (HK89). Apart from this, the X-ray luminosity is systematically higher in Z sources than in atoll sources. Z sources are thought to reach the Eddington limit on the flaring branch, while the luminosity of atoll sources usually does not exceed several 10% L_{Edd} (Van Paradijs et al. 1988). This is supported by the fact that many of the atoll sources show type I X-ray bursts, while X-ray bursts are rarely observed in Z sources (though several were seen in GX 17+2; Sztajno et al. 1986; Kuulkers et al. 1994b and perhaps Cyg X-2 Kahn & Grindlay 1984; Kuulkers et al. 1995). That X-ray bursts occur in Z sources is the only direct indication that these systems contain neutron stars (Lewin et al. 1993).

1.2. Black hole candidates

Another group of X-ray binaries to whose properties those of Cir X-1 have often been compared (and as will become clear below, with good reason), is that of the black-hole candidates (BHCs). Astrophysical black holes are expected to be uncharged and therefore to have no magnetic field. BHCs display a wide range in accretion rates. On the basis of recent work (Miyamoto et al. 1991, 1992, 1993; van der Klis 1994a) it seems likely that the behaviour of black-hole candidates can be described in terms of three states: *low* state, *high* state, and *very high* state. Just as for the neutron stars, the fast-timing properties of BHCs are related to these states. In the *very high state* the power spectra show QPO in the range 2–10 Hz, and band limited noise with cut off frequencies of $\sim$1–10 Hz. In this state rapid changes in the shape and strength of the noise components take place. In the *high state* the power spectra can be well described by a weak power law with an index of $\sim$1–1.5. When a BHC is in the *low state* the power spectra show a strong band limited noise component with a flat top below $\sim$0.1 Hz. The total power in the low state is high (up to $\sim$50% rms), much higher than the total power in the very high and high states.

Black-hole candidates show (perhaps several different kinds of) slower QPO in addition to the very high state 2-10 Hz QPO. In the low and high states QPO and "peaked" band limited noise components with frequencies in the range 0.04 Hz – 1 Hz have been found (for a review, see Tanaka & Lewin 1994). Similarly "slow" QPO have been seen in one atoll source, 4U 1608–52 (Yoshida et al. 1993).

1.3. Neutron star and black hole similarities; where does Cir X-1 fit in?

The fast timing behaviour of some atoll sources when they become very faint resembles that of a BHC in the low state (Inoue 1992; van der Klis 1994b). It has been suggested that the rapid X-ray variability properties of Z and atoll sources and BHCs can be described in terms of three common states, where the 6–20 Hz QPO of Z sources and the 2–10 Hz QPO of BHCs, and also the Z source low-frequency noise, the atoll source high-frequency noise and the BHC low-state and very-high-state band limited noise components are caused by the same physical mechanisms (van der Klis 1994b, c). In this interpretation BHC low states approximately correspond to atoll source island states, and BHC high states to atoll source banana states.

The HK89 classification of neutron star systems in terms of luminosity (L_x) and magnetic field (B), with Z sources at high $L_x$and B, and atoll sources at low L_x and B leaves room for other systems in addition to Z and atoll sources, i.e. systems with high B and low L_x, and systems with low B and high L_x. The former would be Z sources at very low luminosities; no Z source has so far been observed at low intensities. It has been suggested (van der Klis 1991) that Cir X-1 at times is an example of the latter type of system. This suggestion is based on: (i) the presence of type I X-ray bursts; showing that the system contains a low magnetic field neutron star, (ii) the absence of

HBO and periodic pulsations at low L_x, and (iii) the presence of 6–20 Hz QPO (Tennant 1987) at high L_x. If this suggestion were correct one might further expect (van der Klis 1994b) that at high $\dot{M}$ the behaviour would show some similarities to that of BHCs in the very high state, whereas at low $\dot{M}$ the behaviour would be similar to that of atoll sources.

In the light of the above suggestions we studied the fast timing and spectral behaviour of Cir X-1 over its entire range in X-ray flux. For this study we used all *EXOSAT* data of Cir X-1, and made a full, homogeneous analysis in terms of power spectra and CD/HIDs, allowing for a direct comparison with the properties of Z and atoll sources and black hole candidates. Previous work on the EXOSAT data on Cir X-1 concentrated on bursts (Tennant et al. 1986a, 1986b) and QPO (Tennant 1987, 1988a), but did not include a study of the correlations between CD/HID behaviour and the properties of both QPO and noise components in power spectra. We considered to extend our analysis to the properties of time-delays of the noise components for that subset of the data that has spectral resolution combined with high time resolution, but found that at count rates high enough to make statistically significant time delay estimates dead-time induced cross-talk severely hampered the analysis.

2. Observations

Eight observations were made of Cir X-1 with *EXOSAT* over a time span of almost two years. For a log of the observations we refer to Table 1. The total observing time amounts to ~130 hours. We used the data from the medium-energy (ME) experiment (Turner et al. 1981; White & Peacock 1988) on board *EXOSAT*. The present work is constrained to data from the Argon-filled chambers, which are sensitive in ~1–20 keV band.

As a consequence of the long time span over which the observations were performed and the development of new On Board Computer modes during this time, the data have been collected in different modes, thus making a uniform comparison of all data more difficult. Changes in detector efficiencies and gains in the course of time also complicate a uniform reduction of the data. Fortunately, the variations that Cir X-1 exhibits in its X-ray spectrum are so large that we are not impaired much by these instrumental effects, which have consequences on the few % level only. For a review of the changes in the instrument response relevant to this work we refer to Kuulkers et al. (1994a). From that work it can be derived that the systematic uncertainties in the X-ray colours and intensities that we report in this paper are less than 4% over the interval 1983–1986.

The initial version of the software package that we used for the reduction of the data was created at the Laboratorium for Space Research in Leiden; the package was further developed in Amsterdam.

3. Analysis

We constructed colour-colour diagrams (CDs) and hardness-intensity diagrams (HIDs) for each observation. When available we used data with high energy resolution (HER4 and HER5), which were rebinned into four energy channels (2–3, 3–5, 5–7, 7–12 keV). The channels were chosen in such a way that the counts are more or less equally distributed over them. Since Cir X-1 shows large spectral variations this requirement is fulfilled only very approximately (within a factor ~5). Our highest energy boundary is quite low compared to the choices of other authors (e.g. HK89). We note that selecting a higher upper energy bound does not improve the quality of the CDs and HIDs: relatively few counts are added, while background variations become more important. The soft colour is defined as the count rate ratio of the 3–5 keV band to the 2–3 keV band, the hard colour as the count rate ratio of the 7–12 keV band to the 5–7 keV band. The "intensity" as we use it throughout this paper is the observed count rate per cm^2 per second in the 2–12 keV band and has been corrected for background, deadtime and collimator response. Below we will use the symbol C_S for the soft colour and C_H for the hard colour, and I for "intensity".

For the background subtraction we use data that were obtained either just before or just after each observation of Cir X-1, when the satellite was slewing. The background data were inspected to make sure that no sources moved through the field of view of the detector. When the source gets very faint ($\lesssim$0.005 c/s/cm^2), the contribution from the background becomes very important. The galactic ridge (or other point sources) could contribute at most ~0.01 counts $cm^{-2}s^{-1}$ (from Turner et al. 1989, where ~5 mCrab is quoted for the flux from the galactic ridge).

Observation H (day 60 in 1986) did not have data with high energy resolution. For this observation we used high-time resolution data (HER7 mode) to compute the C_S, C_H, and I. These data have four energy channels, which are different from the channels mentioned above, and the lowest of which falls outside the calibrated energy range. For display purposes we corrected the values of the colours obtained in this observation in order to make them correspond better to the other data (see below).

The integration times we used for the time bins in the CDs and HIDs were chosen freely depending on the count rate and on the typical time scales of source variations. When the source count rate was very high 10-second time bins sufficed to obtain reasonable colour estimates, but when the source count rate was very low integration times up to 5000 s were required. We have plotted the light curves of all 8 observations in Fig. 1. The corresponding CDs and HIDs diagrams are shown in Figs. 2, 3, and 4, respectively. In order to allow a comparison between all states of Cir X-1 in the hardness-intensity diagrams, we used a logarithmic scale for I, which for HIDs of Z and atoll sources is usually not necessary.

For the fast timing analysis we performed FFTs of the high time resolution data in order to calculate power spectra. In most cases the time resolution is 8 ms, so the Nyquist frequency is 64 Hz. In general we made FFTs of 256 or 512-s data segments in order to get a good determination of the low frequency part of the power spectrum. All FFTs were made of data at the original time resolution. If a data drop-out occurred during a data segment we excluded it from our analysis, since we found that

Table 1. Observation log of all *EXOSAT* observations of Cir X-1, including the radio phase calculated with the ephemeris of Stewart et al. (1991). Radio phase 0 refers to the onset time of radio flares

Obs. name	Start time yr/day hh mm	End time day hh mm	Net data (s) (approx.)	high-time res. OBC modes	radio phase
A	84/227 05 00	227 15 46	43000	HER6	0.0
B	84/228 05 57	228 22 57	64000	HER6	0.1
C	84/235 15 14	235 19 02	18000	HER6	0.5
D	85/208 20 34	209 19 02	73000	HER7	0.0
E	85/216 20 50	217 11 01	50000	HTR3	0.4
F	85/224 14 39	225 13 25	83000	HTR3, HER7	0.0
G	86/056 11 34	057 10 46	87000	HTR5	0.8
H	86/059 07 59	060 04 02	50000	HER7	0.0

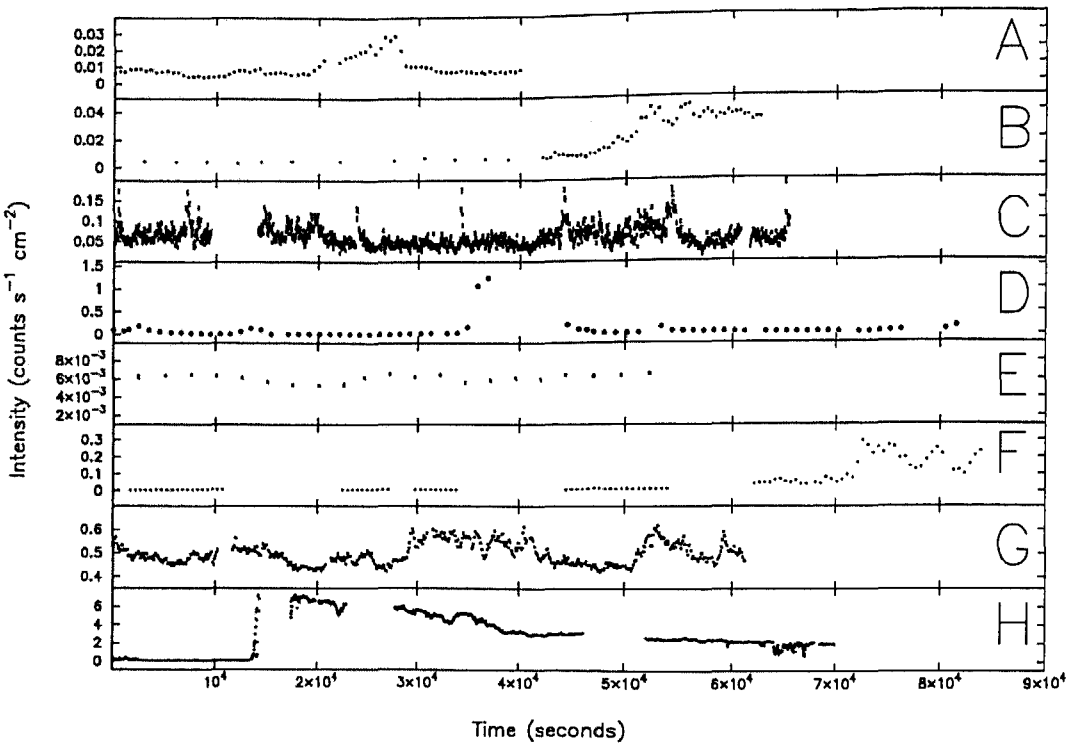

Fig. 1. The light curves of all eight observations. The scale for observation C has been expanded by a factor 4. The true length of observation C is ~18 000 s

substituting the missing data by the mean count rate in general introduced artificial power at low frequencies.

The general procedure we used in the analysis of the power spectrum is based on averaging of the power density spectra obtained from individual data segments. If the source count rate was low, we averaged all the power density spectra of that observation since we were limited by the statistics. If the source count rate was higher we made data selections based on time or position in the CD; this is described in more detail below. Then we fitted simple functional shapes to these average power spectra. We used two different fit models depending on the source flux. When the power spectrum had a power-law shape (that is in all low- and medium state observations and observation G, see Sect. 4.6) an "atoll" model (HK89) consisting of a power-law VLFN component plus an exponentially cut-off power-law HFN component provided satisfactory fits. We found that the HFN component was statistically required during observation G (see Sect. 4.6), but not during the other observations. At high source flux (observation D and H) this model did not fit the data well. There we used a power law plus a Lorentzian centered at zero Hz to describe the noise components, and if QPO were present, a second Lorentzian at the QPO frequency. In Sect. 4 we describe in detail the results of the analysis of the power spectral shapes in all states.

The so-called Poisson level of the white-noise component induced by the photon counting statistics was predicted from the count rates corresponding to each individual FFT using the knowledge of *EXOSAT* dead-time processes (Andrews & Stella 1985). It was subtracted from the power spectrum before averaging the power spectra. For the HER7 mode data, we find that we

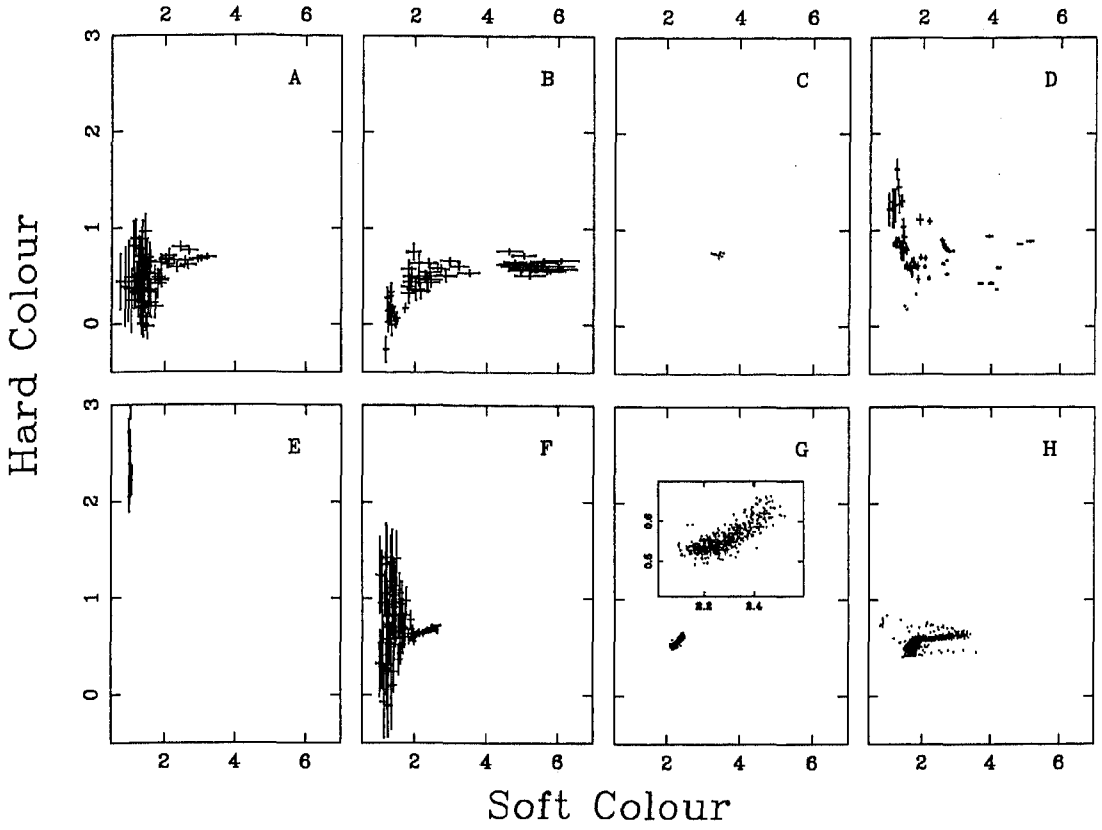

Fig. 2. The colour-colour diagram of all eight *EXOSAT* observations of Cir X-1. The horizontal scale is the soft colour, which is defined as the count rate ratio between the 3–5 keV and 2–3 keV band. Vertical scale is the hard colour, defined as the count rate ratio between the 7–12 keV and 5–7 keV band. Count rates have been corrected for dead time effects. The letters identifying the observations are indicated in the top right of each panel (see Table 1). For clarity no error bars have been plotted for observations C, G, and H; their size is comparable to the smallest error bars in e.g. observation D

can predict the Poisson level from the count rate (using Eq. 3.11 from van der Klis 1989b with a sampling interval of 1/3569 s) with a relative accuracy of better than ~1% up to ~1300 c/s. At higher count rates the prediction of the Poisson level becomes gradually less accurate (the error is ~10% at 2000 c/s); we then use the empirical relation between the observed intensity and the actual Poisson level found by Kuulkers et al. (1994a) to determine the Poisson level. For the HTR3 and HTR5 data modes (which are not affected by dead-time processes in the on-board computer of *EXOSAT*) we find that we can predict the Poisson level (using Eq. 3.9 in van der Klis 1989b with a dead time of 5.5 μs) with an accuracy of better than $\sim 10^{-3}$ for our highest count rates in this mode. For lower count rates this accuracy gets better (Berger & van der Klis 1994). We use the mean count rate per power spectrum to determine the Poisson level. During the large flare in observation D we found that the predicted Poisson levels were no longer entirely reliable. We then introduced the Poisson level as an additional free parameter in our fits. In this way we found a lower than predicted Poisson level (which can not be caused by an unknown component in the power spectrum, since this can only increase the apparent Poisson level).

All power spectra were normalized according to the normalization used by Belloni & Hasinger (1990) and Miyamoto et al. (1991), which gives the power density in units of (fractional rms)^2/Hz or (rms/mean)^2/Hz. This normalization is obtained by dividing a "Leahy-normalized" power spectrum (Leahy et al. 1983) by the count rate and performing a correction to background-corrected fractional rms. The advantage of this normalization is the easy comparison of power spectra at different flux levels in terms of fractional rms. The disadvantage is the less straightforward estimation of the significance of narrow peaks in the power spectrum.

4. Results

In this section we describe in detail the results of the power spectral fits and their relation to the CDs and HIDs. In all observations, we selected power spectra on the basis of time and position of the source in the CD/HIDs in order to obtain information about the changes of power spectral shape as a function of other source characteristics. The power spectra of the low flux (<1 c/s/ cm^2) data observations A, B, C, the non-flare part of D (<3 10^4 s and >5 10^4 s in Fig. 1), E, F, G, and the part of H before the intensity step (<1.4 10^4 s) could in all cases be fitted satisfactorily with an atoll model. The fit parameters can be found in Table 2 and the power spectra are shown in Figs. 5,

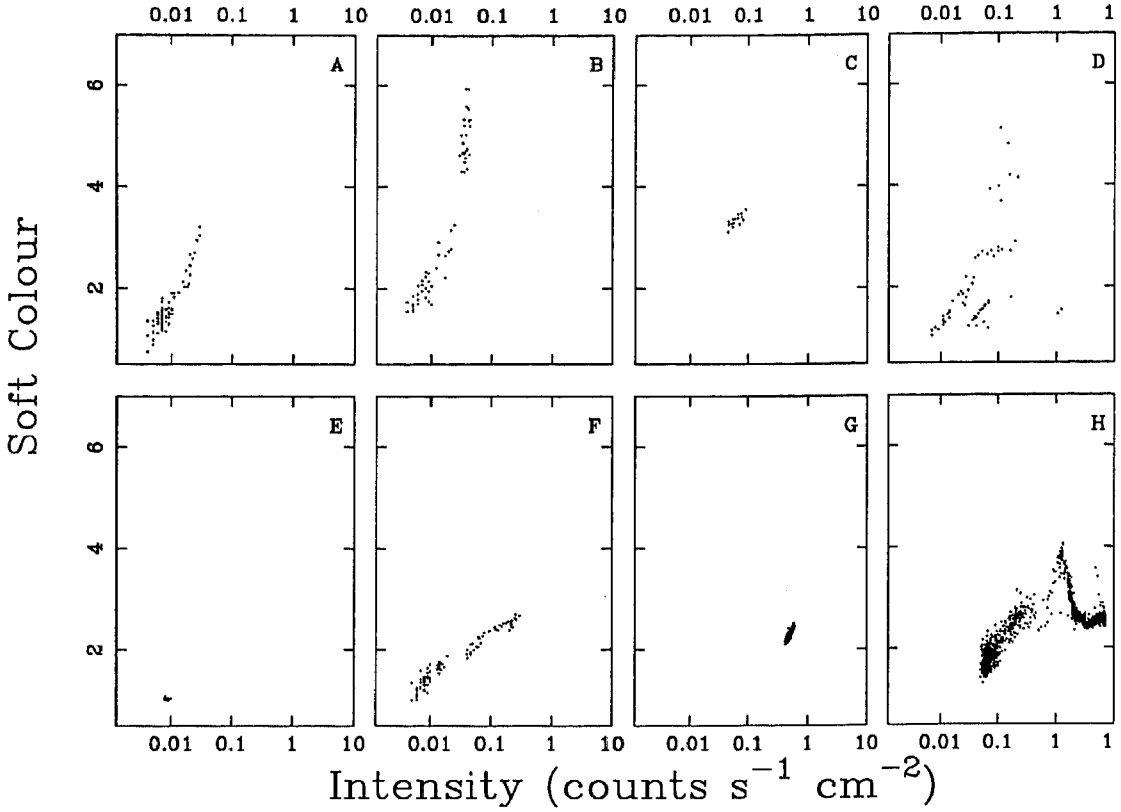

Fig. 3. The intensity vs. soft colour diagram for Cir X-1. The horizontal scale is the intensity in the 2–12 keV band in units of counts cm^{-2}s^{-1}. Count rates have been corrected for dead time effects and collimator response. The vertical scale is the soft colour, defined as the count rate ratio between the 3–5 keV and 2–3 keV band. Count rates have been corrected for dead time effects and collimator response. The observation dates are indicated in the top right of each panel

6, and 7. For the high intensity states where the flux reached levels in excess of 1 c/s/cm^2, i.e. the big flare in D (between 3 10^4 s and 5 10^4 s), and the post-step part of H (>1.4 10^4 s), the power spectra required more complicated fit functions. The fit results for the flare in D can also be found in Table 2, and for the part of H after the step in Table 3 and Fig. 8. Below we quote binary phases for each of the observations based on the ephemeris of Stewart et al. (1991), with an rms error of 0.06 d, which is based on radio observations contemporaneously with our X-ray observations.

4.1. The 1984 observations on day 227 and 228 (A and B; phases 0.0 and 0.1)

During observations A and B, which took place on consecutive days near phase zero, the intensity is at a very low to low level (0.003–0.04 counts cm^{-2}s^{-1} in the 2–12 keV band; as noted above, we are using this band throughout the paper when we refer to intensities and count rates). In observation A, there is a small flare up to 0.03 counts cm^{-2}s^{-1}. Towards the end of observation B, around phase 0.1, the intensity rises to 0.04 counts cm^{-2}s^{-1}.

The CDs and HIDs show substantial variations in both colours and intensity. When the source intensity increases the soft and hard colours both increase. At the highest intensities the hard colour does not increase further, while the soft colour does. The scatter in the left parts of CD and HIDs (soft colour below ~1.5 and intensity below ~ 0.01 counts cm^{-2}s^{-1}) is mainly statistical, and due to the low count rates there. The tracks in the diagrams are consistent with being identical between the two observations.

The power spectra can be well described by only a power-law component. The rms amplitude (0.001-1 Hz) of the best-fit power law ranges from 5 to 12 % and possibly increases when the flux increases, while the power-law index remains constant near 1.5–1.6. There seems to be some excess power with respect to the best-fit power law in the >1 Hz range (see Fig. 5) but this is caused by the logarithmic power scale, which makes small and negative (after subtraction of the Poisson level) powers invisible; the excess is not statistically significant.

4.2. The 1984 observations on day 235 (C; phase 0.5)

Observation C took place at mid-phase about a week after observations A and B. The source is brighter (0.02–0.25 counts cm^{-2}s^{-1}) than during observations A and B and although the intensity varies considerably, there is little variation on time scales longer than a few 1000 s. In the CDs and HIDs we see

Table 2. Power law fits to power spectra of all observations

Obs.	Intensity cnts/s/cm^2	α	rms in % (0.001–1Hz)	HFN rms (%) (1-100 Hz)	HFN index	HFN cut-off (Hz)	χ^2/d.o.f.
A	1.2×10^{-2}	$1.29^{+0.38}_{-0.27}$	$8.8^{+2.4}_{-1.9}$				42.1/36
B (low)	8×10^{-3}	$1.90^{+5.0}_{-0.27}$	$5.3^{+4.0}_{-2.2}$				31.6/36
B (high)	3×10^{-2}	1.47±0.10	$12.5^{+0.62}_{-0.64}$				28.0/36
C	5×10^{-2}	1.12±0.01	56.7±1.0				60.0/68
D (before first flare)	1.5×10^{-2}	2.2±0.4	13.8±1.9				49.2/42
D (before big flare)	1×10^{-2}	1.8±0.2	28±2				34.4/39
D (first flare)	0.2	1.15±0.03	33±1				72.2/68
D (last flare)	0.1	1.2±0.3	$7.4^{+1.6}_{-1.1}$				38.8/39
E	6×10^{-3}	0.9 [a]	$2.4^{+7.5}_{-8.5}$				36.8/39
F (low)	1×10^{-2}	$1.20^{+0.97}_{-0.35}$	$2.4^{+7.5}_{-13.3}$				35/39
F[c]	0.12	0.91±0.07	28.5±1.5				40.5/50
F[d]	0.15	1.02±0.03	22.3±0.8				64.6/50
G (tot)	0.50	1.83±0.05	3.6±0.1	1.8±0.2	$-0.86^{+0.54}_{-0.89}$	$3.3^{+2.0}_{-1.1}$	49.1/38
G (low)	0.43	1.80±0.1	2.3±0.2	2.1±0.3	$-3.1^{+1.8}_{-10.8}$	1.6±2.1 [b]	57.5/38
G (med)	0.51	1.87±0.08	3.1±0.2	2.0±0.4	$-0.5^{+0.4}_{-0.8}$	$6.6^{+5.8}_{-3.0}$	37.3/38
G (high)	0.58	1.92±0.08	4.3±0.3	1.7±0.3	$-0.2^{+0.3}_{-0.6}$	$3.5^{+2.6}_{-1.9}$	58.0/38
H[e]	0.3	1.58±0.05	$34.9^{+3.6}_{-2.8}$				36.7/50
H[f]	8×10^{-2}	2.0±0.3	23^{+13}_{-5}				20.9/13

[a] No error scan possible; see also text
[b] Error is error in positive direction; no error scan in negative direction possible
[c] Low part after burst 1; 11000 seconds of data
[d] Between bursts 2 and 3; 5000 seconds of data
[e] first 2500 seconds of data; medium flux
[f] between 2500-12500 seconds of data; low flux

Obs.	Intensity cnts/s/cm^2	FWHM (Hz)	rms in % (0.001–10Hz)	QPO rms (%)	QPO freq. (Hz)	QPO width (Hz)	χ^2/d.o.f.
D (big flare)[g]	1.2	0.008±0.002	35^{+1}_{-8}	2.1±0.4	1.40±0.02	0.015±0.001	331/306

[g] Fitted with zero-centered Lorentzian

Table 3. Fits to the power spectra obtained during observation H and selected according to the boxes drawn in Fig. 10. No satisfactory fit was possible to power spectra No. 2 (see also Fig. 8)

No	rms VLFN (%) 0.01–1 Hz	α	rms Lor. (%) 0.01–100 Hz	FWHM Lor. Hz	rms QPO %	QPO FWHM Hz	QPO freq Hz	χ^2/dof
1	$21.6^{+8.2}_{-7.8}$	$2.71^{+0.37}_{-0.46}$	$4.12^{+1.03}_{-1.08}$	$27.7^{+20.8}_{-15.9}$	–	–	–	46.5/48
3	0.98±0.06	$1.62^{+0.23}_{0.19}$	7.35±0.08	$33.2^{+1.2}_{-1.1}$	–	–	–	117.5/48
4	$0.95^{+0.10}_{-0.08}$	$2.00^{+0.42}_{-0.30}$	7.06±0.08	31.4±1.1	–	–	–	62.0/48
5	$1.23^{+0.16}_{-0.28}$	$0.69^{+0.67}_{-0.16}$	$6.27^{+0.58}_{-0.78}$	$21.9^{+2.1}_{-3.4}$	$2.89^{+0.26}_{-0.27}$	$2.01^{+0.53}_{-0.60}$	9.28±0.13	40.2/45
6	$1.31^{+0.13}_{-0.16}$	$0.44^{+0.04}_{-0.06}$	$3.65^{+0.16}_{-0.15}$	$4.9^{+0.7}_{-0.6}$	4.88±0.13	$3.20^{+0.19}_{-0.20}$	8.38±0.06	41.3/45
7	2.23±0.11	0.73±0.03	2.95±0.16	$2.7^{+0.5}_{-0.4}$	5.32±0.15	$4.16^{+0.23}_{-0.25}$	6.98±0.09	73.7/45
8	$4.98^{+0.14}_{-0.11}$	$1.14^{+0.07}_{-0.06}$	$3.36^{+0.60}_{-0.74}$	$9.4^{+1.6}_{-1.0}$	$4.26^{+0.08}_{-0.17}$	$1.82^{+0.07}_{-0.09}$	$5.60^{+0.04}_{-0.03}$	146.5/45
9	$7.7^{+1.7}_{-1.3}$	$1.86^{+0.55}_{-0.37}$	$3.67^{+0.67}_{-1.14}$	$1.6^{+1.0}_{-0.8}$	$5.12^{+0.43}_{-0.42}$	$2.19^{+0.58}_{-0.49}$	$5.84^{+0.23}_{-0.21}$	55.1/45
10	$11.2^{+1.9}_{-1.8}$	$2.05^{+0.24}_{-0.23}$	$4.32^{+0.75}_{-0.82}$	$5.1^{+4.6}_{-2.2}$	$4.42^{+1.52}_{-0.35}$	$0.47^{+0.44}_{-1.38}$	$5.78^{+0.05}_{-0.10}$	36.2/45
11	$7.7^{+4.4}_{-2.1}$	$1.73^{+0.64}_{-0.45}$	–		$6.44^{+0.81}_{-0.75}$	$1.36^{+0.85}_{-0.74}$	$5.69^{+0.18}_{-0.31}$	38.8/47

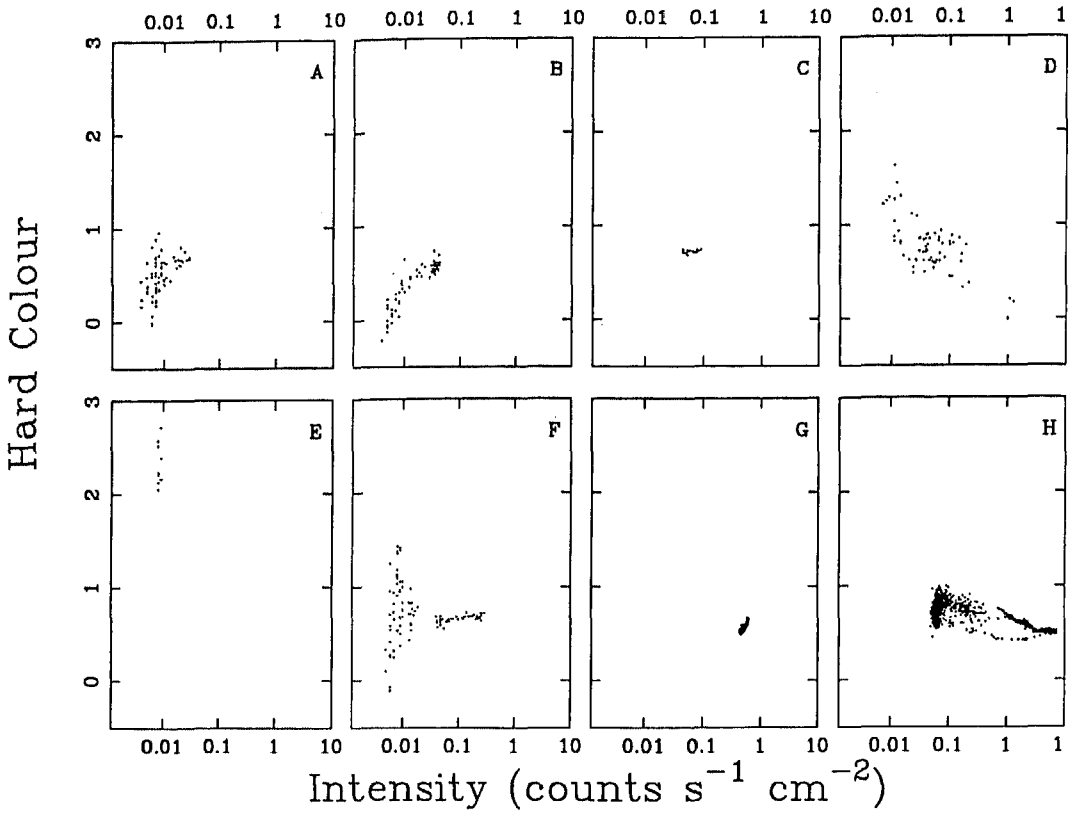

Fig. 4. The intensity vs. hard colour diagram. Same as Fig. 2, except that the vertical scale is the hard colour (count rate ratio in 7–12 keV and 5–7 keV band)

relatively little variation. The soft colour varies in correlation with the intensity between 3.2 and 3.6, the hard colour stays almost constant at a value of 0.8.

The most striking feature during this observation is the presence of peculiar bursts or flares with a recurrence timescale of $\sim$ 2000 s, which each last for a $\sim$100 s. The highest of these bursts have been previously reported by Tennant et al. (1986a), but they only seem to be the top end of a distribution of bursts of various peak fluxes. This distribution may be bimodal, as 8 bursts had high peak fluxes (>0.15 c/s/cm^2), many had low fluxes (<0.08 c/s/cm^2) and 4 had intermediate fluxes. In Fig. 9, we show a portion of the light curve, where apart from two large bursts (both reported by Tennant et al. 1986a) many smaller bursts can be seen.

The bursts cause a very strong power law component in the power spectrum, with an index of 1.12±0.01 and an rms amplitude (0.001–1 Hz) of $\sim$50% (this value decreases to $\sim$25% for parts of the data which do not contain strong bursts, while the slope does not change). Tennant et al. (1986a) already raised the question whether the eight strong bursts are type I X-ray bursts or not, and commented on their unusual (for type I bursts) X-ray spectral properties. The time intervals between the eight bursts are short (eight bursts in $\sim$20 000 s). Smaller recurrence time scales have occasionally been found in X-ray burst sources (see Lewin et al. 1993), but 2500 s is shorter than usually usually encountered, for a large number of consecutive bursts. That the bursts appear to be a part of a distribution involving many much smaller events provides an argument that it is unlikely that they are type I bursts.

In the observation which was reported by Toor (1977), the source showed spikes on a short time scale. This observation was obtained at radio phase $\sim$0.4. This could be reminiscent of the fast variability behaviour we found during observation C, where an enormous amount of power was present and the distribution of counts per bin is clearly non-poissonian.

4.3. The 1985 observations on day 208-209 (D; phase 0.0)

Observation D, near phase zero, shows large variations in the intensity, ranging from very low to high (0.005–1.2 c/s/cm^2). The light curve contains several small flares and a very big one (each lasting several thousand seconds); between these flares the flux drops to a very low level. In the big flare the source reached such a high count rate that the on-board computer of *EXOSAT* crashed. This explains the gap during the highest part of this flare.

The variation in the CD/HIDs during this observation is large: the soft colour varies between 1 and 5, the hard colour between 0.3 and 1.6. The soft colour is highest when the intensity is large, with the exception of the highest flux levels, in the flares, when the soft colour falls back to $\sim$1.6. The hard colour is roughly anticorrelated with the flux. The tracks in the CD

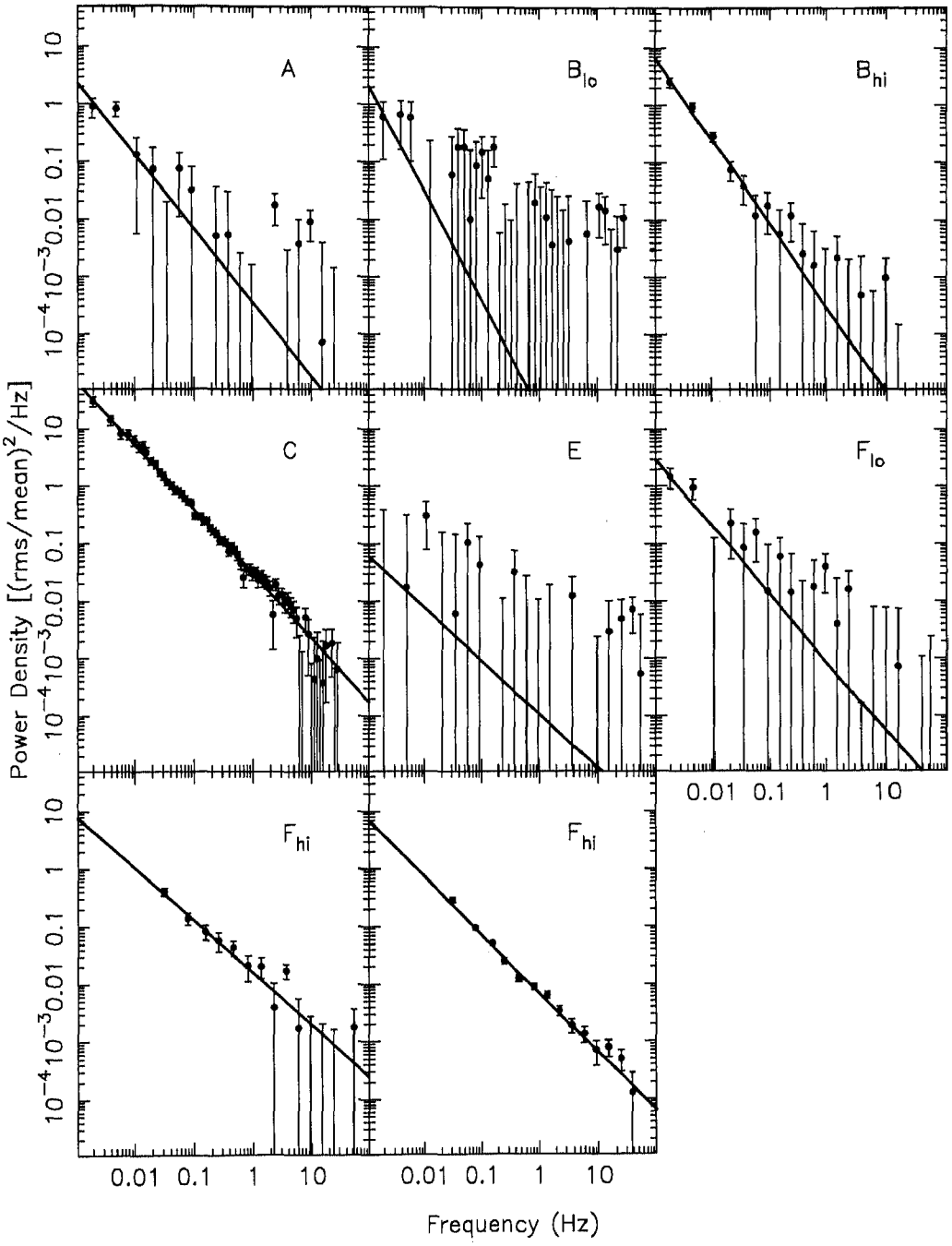

Fig. 5. A collection of the power spectra of Cir X-1 during different observations. All power spectra have their Poisson level subtracted and the vertical scale is the power in units of (rms/mean)^2/Hz. In the upper row we see power spectra from observation A, B (low count rates), B (higher count rates). The fit to the second spectrum seems to be quite bad, this is due to some negative points near 0.01 Hz, however the χ^2/d.o.f. is good (see Table 2). In the middle row the power spectra obtained during observation C, E, and F (low count rate part) are plotted. In the lower part of the figure spectra obtained during the high flux part of observation F are plotted (corresponding to the spectra described in Table 2)

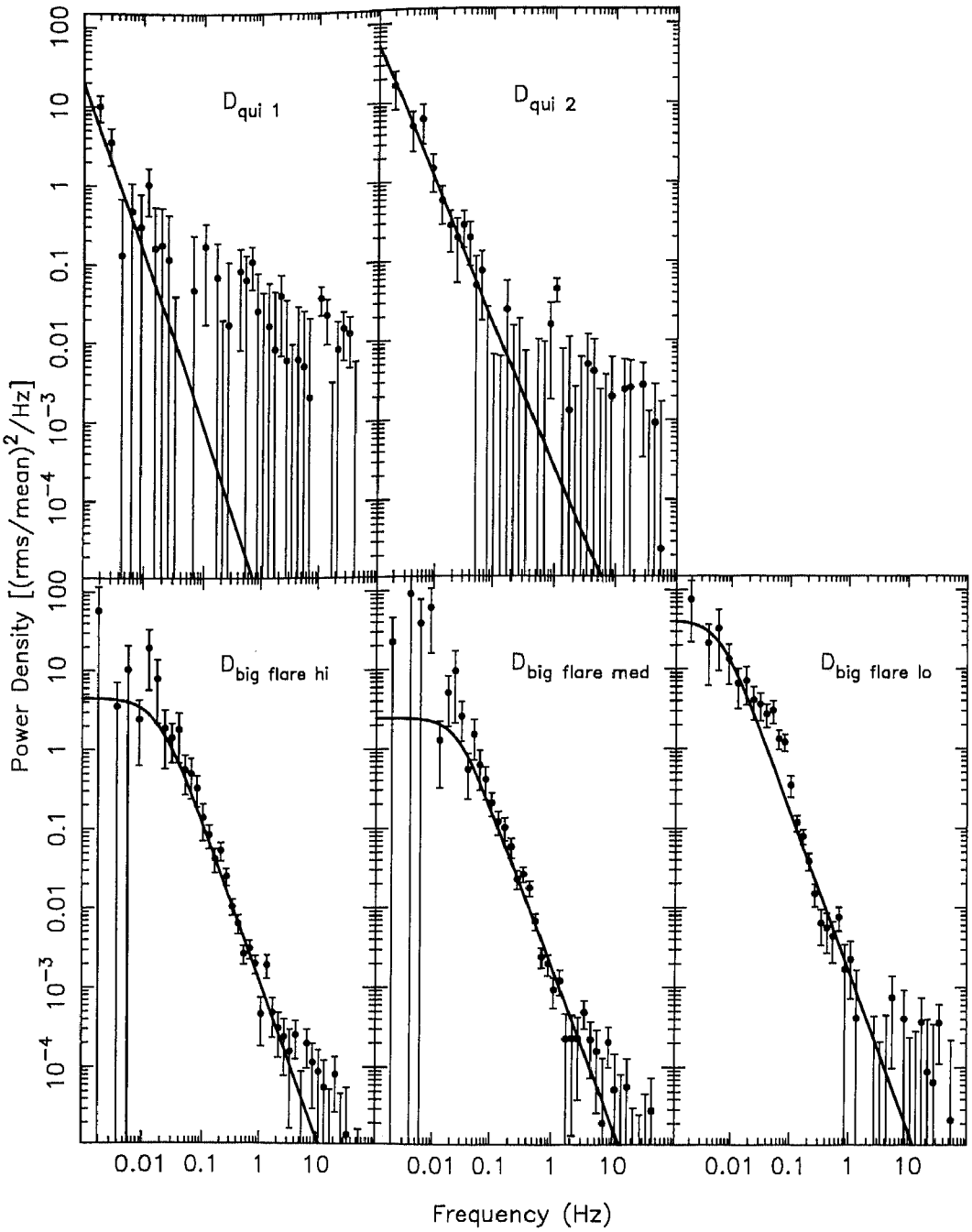

Fig. 6. A sample of the power spectra obtained during observation D. In the top part two power spectra obtained during a low parts of the observation are plotted. In the bottom power spectra obtained during different flux levels during the big flare are plotted

and the soft HID during different flares are not the same, which cause complex patterns in these diagrams.

During the big flare the source is highly variable on a time scale of $\sim$ 10 s. The power spectrum (Fig. 6) has a very strong noise component (up to 40% rms between 0.001 and 10 Hz, which can not be described with a single power law fit. We find that a Lorentzian centered at zero Hz with a FWHM of $\sim$0.03 Hz gives a much better fit (see Table 2 for the fit parameters). The apparent excess power visible above $\sim$2 Hz is not significant. During the big flare 1.4 Hz QPO are present (see Fig. 6) which have already been discussed in some detail by Tennant (1988a). During two smaller flares near 2000 s and 80000 s, which reached count rates of 0.15 c/s/cm^2, the power spectrum has a power-law shape with an rms ranging from 7% to 33%, with an index of $\sim$1.2. In between the flares the power spectrum shows only a very weak power law component.

The 1.4 Hz QPO which was found earlier Tennant (1988a) causes a small peak (FWHM $\sim$ 0.02 Hz) in the power spectrum.

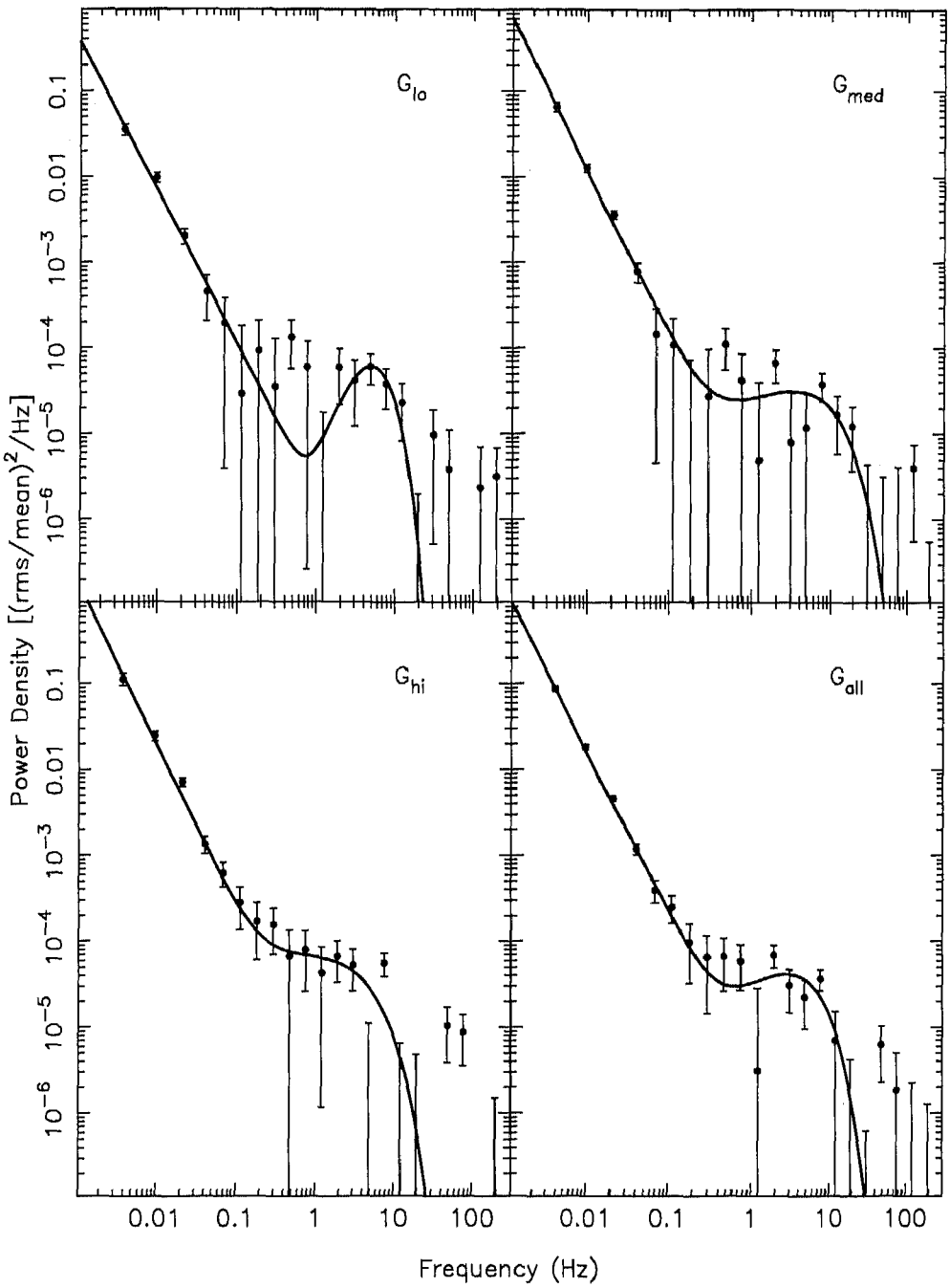

Fig. 7. The power spectra as obtained during obervation G. The top left panel is the spectrum obtained at the lowest count rates. The spectrum obtained at medium count rates is plotted in the top right panel. The bottom left panel shows the spectrum as obtained at the highest count rates. The bottom right panel shows the total power spectrum obtained from the total data set

It is interesting to note that during the discovery of Cir X-1 evidence for power at 1.4 Hz was also found (Margon et al. 1971). In these observations the peak also had a small width. This was originally interpreted as evidence for a pulsating X-ray source. If one calculates the orbital phase using the ephemeris given by Nicolson (1980) one finds that at the time of discovery the orbital phase was 0.1 (with an estimated error of ~0.1). The 1.4 Hz QPO discovered by Tennant (1988a) was found at approximately the same phase (0.0).

4.4. The 1985 observations on day 216 (E; phase 0.4)

During mid-phase observation E (one week after observation D) we encountered Cir X-1 in a persistent very low state (below ~0.007 c/s/cm^2). As noted in Sect. 3, at such low count rates the contribution of the background becomes very important. From

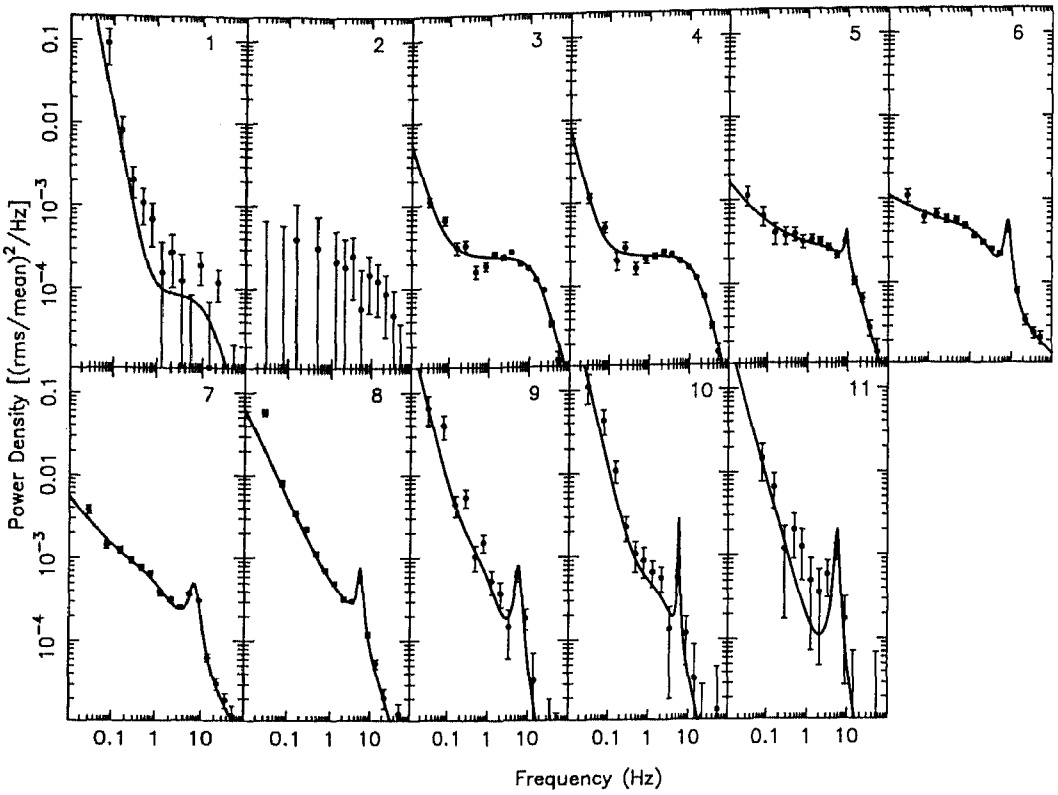

Fig. 8. A collection of power spectra when the source moves through the CD during the observation on day 60 of 1986. See Fig. 10 for the positions in the CD where the power spectra are obtained. The numbers in the upper right corner correspond to the numbers in Fig. 10

the variations in the light curve (Fig. 1) we see that, assuming that the background is constant, at least 20% of the flux must be from Cir X-1 itself.

The colours in this observation are different from those during the other observations: at low energies the spectrum is very soft ($C_S \sim 1$), while at higher energies it is very hard ($C_H \sim 2 - 2.5$). This is probably not caused by errors in the background subtraction, or the contribution from the galactic ridge since in other low state observations we do not see a hardening of the spectrum at low count rates. This argues in favour of the possibility that during this observation the spectrum of Cir X-1 is different.

There are not enough source counts to make a good estimate of the fractional rms source variability: we find an rms (0.001–1 Hz) of $2.4^{+7.5}_{-13.4}$%. The slope of the power-law fit to the power spectrum is 0.93. However, the power spectrum is consistent with zero power; this gives a χ^2 of 36.8 with 41 dof.

4.5. The 1985 observations on day 225 (F; phase 0.0)

During most of observation F, which took place near phase zero, one binary cycle after observation D, the intensity is low (< 0.02 c/s/cm^2) and rising very slowly; about 20 000 s before the end of the observation it rises rapidly from a low flux level to a high flux level (0.01 to 0.3 c/s/cm^2). At the end of the observation three X-ray bursts occur (not visible in Fig. 1 because of the low time resolution). They are typical of type I bursts (Tennant et al. 1986b).

When the flux increases the C_S also increases, while C_H increases by a much smaller amount. At the highest flux level the colours are comparable to those during observation G (see below). The scatter in the hard colours at low intensities (in the left part of the CD) is statistical: there are few counts in the hard energy bands.

The power spectra can be well described by a power-law with an rms which increases when the flux increases. The rms amplitude (0.001-1 Hz) ranges from less than 10% at the lowest flux levels to 30% at the highest flux levels. The slope ranges from 0.9 to 1.2 (see Table 2). The bursts are not included in these power spectra.

4.6. The 1986 observation on day 56 (G; phase 0.8)

Observation G is the only observation that took place well past mid-phase but not near phase zero. The light curve for this observation shows that the source is in a relatively bright state (0.42–0.60 counts cm^{-2}s^{-1}), where the flux varies relatively little (less than 30% during the entire observation).

The CD shows a curved branch on which both colours increase with flux. The range in colours during this observation is small compared to the overall changes seen in Cir X-1, but comparable to changes found in, for instance, atoll sources in

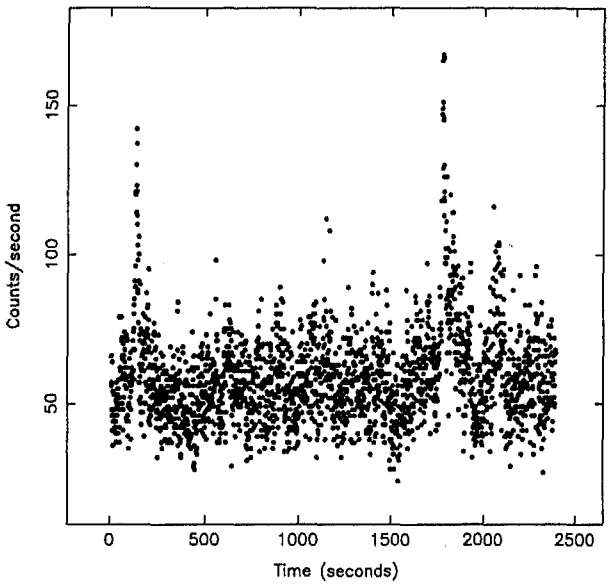

Fig. 9. Part of the light curve of observation C in more detail. We can see not only the large bursts, but also may many smaller ones. Points are 0.93 s averages

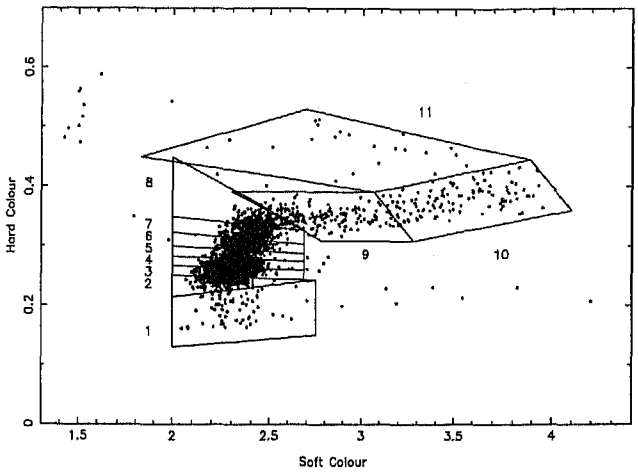

Fig. 10. In this figure a blow up off the CD during observation H (see also Fig. 2) is presented. In this figure the areas are drawn which are used to select to power spectra. The numbers in this figure can be used to find the corresponding power spectrum in Fig. 8

the banana state. The soft colour varies between ~2 and ~2.5, the hard colour between ~0.5 and ~0.65.

The power spectra show a weak VLFN component with an *rms* variation of a few % ranging between 2.4% and 4.2% from low to high count rates, while the power law index changes from 1.80 to 1.92 (also from low to high count rates). The power spectra also show evidence for a HFN component (see Fig. 7). In the power spectrum of the total data set an F-test for additional terms (3 parameters which describe the HFN) gives a probability of 0.11% (corresponding to $\sim 3.2\sigma$) to exceed the found decrease in χ^2. In the three power spectra which were selected on the basis of C_S (less than 2.22, between 2.22–2.32, and more than 2.32) the HFN component was present with a significance ranging from $\sim 2.2 - 2.5\sigma$. The parameters of this component can also be found in Table 2.

4.7. The 1986 observations on day 59-60 (H; phase 0.0)

The light curve for observation H, which was done at phase zero, four days after observation G, shows a low level part after which a very sharp rise ("step") to a very high flux is observed, from 0.01 to 7 c/s/cm^2 (0.9-9.7 keV) within 500 s. After this step the intensity more or less gradually, but with considerable variations, drops to a level of 1.9 c/s/cm^{2}at the end of the observation.

In the CD there is a clear track that appears after the sharp rise and has two sharp bends (Fig. 10). Before the rise when the intensity is low, the source is in the top left part of the CD; they are more clearly visible in the HIDs. After the step the source is in a different position in the CD. It first follows a branch in the CD (Fig. 10) where C_S slightly increases from ~2.3 to ~2.5, while C_H increases from ~0.2 to ~0.35. Then there is a sharp bend to the right, where C_H increases to ~4 and C_S increases more slowly to ~0.4. An ill-developed third branch can be seen above this almost horizontal branch, which occurs at the end of the observation when the count rate "dips".

It is difficult to compare this CD to that during other observations, because in observation H the available energy bands (from the HER7 mode, see Sect. 3) are different. Therefore we made a CD of observation G using the same energy bands as in observation H. Comparison with the CD of observation G in our "standard" energy channels, shows that (to first order, neglecting the "colour-dependent" term in the conversion) we can convert the colours using the conversion: $C_{S\,\mathrm{standard}} = C_{S\,\mathrm{HER7}} - 0.60$ and $C_{H\,\mathrm{standard}} = C_{H\,\mathrm{HER7}} + 0.25$, where the indices HER7 stand for colours obtained with the "HER7" mode data and "standard" for colours obtained with the energy bands which are used with the other observations. The CD and HIDs of observation H in Figs. 2, 3, and 4 have been corrected in this way.

The shape of the power density spectra changes considerably as the source moves in the CD. We have selected power density spectra on the basis of the position of the source in the CD (see Fig. 10, where boxes are drawn to indicate the data sets for which the average power spectra have been obtained). In Fig. 9 we present the corresponding average power spectra. During the gradual decline a very distinct QPO peak (Tennant 1987) becomes visible in the power spectra (~7 hrs after the maximum flux), whose frequency changes from ~ 17 Hz to ~ 5 Hz. Table 3 contains the results of the fits to these power spectra. In this table the highest frequency is substantially less then 17 Hz; this is caused by the fact that the high frequency QPO is found during the highest fluxes. Due to data drop-outs there it was not possible to make FFTs of long enough data segments, which were required to get an indication of the low-frequency part of the power spectrum.

The *Ginga* observations reported by Stewart et al. (1991) are similar to our observation H with respect to the global shape of the light curve and the radio phase at which the observation

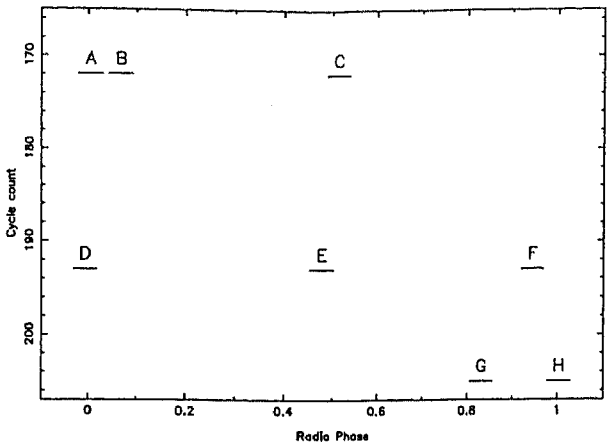

Fig. 11. In this figure the radio phase and epoch of the observations are plotted. Along the horizontal axis the radio phase is indicated, while the vertical axis is the cycle number (both are calculated using the ephemeris of Stewart et al. (1990). The length of the lines indicating the times of the observations are approximately equal to the observing time, with the exception of observation C which is ~5 times as short

was obtained. In the same observation QPO with a frequency similar as found in observation H was detected by Makino et al. (1992). All together this observation seems to have the same properties as observation H, but took place a little over 3 years after our last observation. It could be that the viewing geometry of the source was similar to that during observation H, which is consistent with a long term variation in the geometry.

5. Discussion

A wide variety of power spectral and CD/HID behaviour is seen in Cir X-1, but we find that some general patterns emerge when the phenomenology is considered jointly as a function of binary orbital phase, X-ray intensity and epoch.

Let us first consider the properties of the source as a function of *orbital phase* (see Fig. 11). There are clear differences between the observations near phase zero and the mid-phase observations: all phase zero observations show a large range in colour and intensity, whereas in the two mid-phase observations where Cir X-1 is bright enough to reliably measure the colours (observations C and G) there is very little variation in either colours or intensity (Figs. 2–4). The observations near phase zero tend to show changes in overall brightness by at least an order of magnitude on time scales of 10^{3-4} s, whereas in the mid-phase observations E and G the intensity did not vary by more than 30%. In mid-phase observation C the peculiar flares occurred that were described in Sect. 4.2; the largest of these increased the flux by a factor of ~10, but they never lasted longer than ~500 s.

Now consider those observations that took place at the same phase as a function of *X-ray intensity*. The observations at phase zero with count rates <1 c/s/cm^2 (observations A, B, D non-flare, F, H pre-step) all show power spectra that fit a power-law shape with an index 1–1.6 and a fractional rms amplitude of 5–35% that increases with source flux. The behaviour of the source in the CD/HIDs during these observations is also similar, except for observation D, where each flare seems to create its own track in the CD/HIDs.

In the two high count rate (>1 c/s/cm^2) intervals (D big flare and H post-step; both occur near phase zero) the pattern becomes more complex. In observation D the big flare is quite soft, while in observation H a complex but approximately one-dimensional track containing several sharp bends shows up in the CD. The "branches" delineated by these bends are somewhat reminiscent of those seen in Z sources. At these high fluxes the power spectra are more complex as well, which may partly be due to the higher sensitivity at these high count rates to weak power spectral components. The power spectra show QPO and band limited noise components.

Finally, let us consider the source properties as a function of *epoch*, in particular, *year of observation*. It is clear from the above that we should only compare observations that were obtained near the same orbital phase. When we compare the character of the phase zero observations in 1984, 1985 and 1986, we see that the source flares up to higher and higher levels of ~0.03–0.04, 1.2, and 7 c/s/cm^2, respectively. The mid-phase observations do *not* show such a simple pattern, as in consecutive years (observations C, E, G) the flux levels are ~0.1, ~0.005, and ~0.5 c/s/cm^2, respectively.

5.1. The general picture

The large flares and intensity steps that occur near phase zero have been previously explained in terms of an eccentric binary model, where periastron, and consequently increased mass transfer, occurs near phase zero (Murdin et al. 1980). We shall adopt this model in our further discussion.

It then seems reasonable to hypothesize that the following scenario applies: near phase zero, in periastron, a large (perhaps super-Eddington) mass transfer takes place from the companion star to the vicinity of the neutron star. A disk either forms or gets replenished with a large amount of newly transferred matter, and accretion at a high rate begins taking place. During these phase-zero episodes *the accreting matter can obscure our line of sight* towards the neutron star. There are at least two regions where such obscuration could occur: the inner disk, which at near-Eddington accretion rates may become geometrically thick, and the outer disk and accretion stream, which can be expected to be in great turmoil due to the relatively sudden onset of accretion on approach of periastron. Consequently, the phenomenology near phase zero will be determined by a combination of near- and super-Eddington accretion and obscuration of the central source by matter that is being transferred in a non-stationary fashion. These two unstable processes could explain the wild variations in X-ray flux observed near phase zero.

At later phases in the binary cycle, mass transfer from the companion to the neutron star's vicinity ceases, and what remains is a disk that gradually empties itself onto the neutron star, a quieter process that leads to less extreme brightness variations. The character of the emission at mid-phase would in

this scenario depend to a large extent on the properties of the disk that is built up in the previous phase-zero episode. In our observations there is no clear correlation between the source brightness at mid-phase and that at the previous phase zero. This then would imply that *obscuration* effects must dominate what we see at phase zero. In the following, we first discuss a possible explanation for the gradual evolution in brightness and, by hypothesis, obscuration effects that we observe in our phase zero observations in subsequent years. We then compare our observations to those of other low-magnetic field accreting compact objects. We point out some striking similarities in the behaviour of Cir X-1 with atoll sources, Z sources and BHCs. We then disccuss to what extent similarities in the physical processes that occur in these sources and in Cir X-1 might underlie these phenomenological similarities.

5.2. A long-term change in the behaviour of Cir X-1?

In the previous section we noted that in our observations there is a gradual increase in the brightness of Cir X-1 near phase zero from 1984 to 1986. We further argued that obscuration must be a main determinant of the source flux near phase zero. We here discuss a model that could explain that in the course of the years 1984–1986 the obscuration in the line of sight towards the central object decreased, namely, apsidal motion of an eccentric orbit, which was first suggested by Murdin et al. (1980). The model of Murdin et al. (1980) assumes an early-type ($\sim 20\,M_\odot$) star as a companion. For this companion and an eccentricity of 0.8 Murdin et al. (1980) found that the apsidal motion period is between ~7 and ~400 years. However, it is more likely that the companion is a Roche-lobe filling low-mass star with a mass between 0.7 $M_\odot$–1.4 $M_\odot$ (i.e. a mass-ratio q=0.5–1). We assume an apsidal motion constant k of 0.14 (appropriate for a fully convective star, Kopal 1959). Using the equation (Batten 1973):

$$P/P_{\rm aps} = k(\frac{M_{\rm X}}{M_\star}(15f + g) + g)(\frac{R_\star}{a})^5 \qquad (1)$$

where $f(e) = (1 - e^2)^{-5}(1 + 3e^2/2 + e^4/8)$ and $g(e) = (1 - e^2)^{-2}$, $M_{\rm X}$ is the mass of the compact object (1.4 $M_\odot$), $M_\star$, $R_\star$ are the mass and radius of the companion, and a is the orbital separation, we find that for an eccentricity e of 0.7–0.8 (this value is taken from Murdin et al. 1980, but the obtained value of the period is only slightly dependent on e) the apsidal motion period is between 2 and 4.5 years. This means, that in the 1.5 year span of our observations a large change in periastron angle could have occurred. Consequently, the position angle under which we see the system at phase zero would have changed considerably in that time. This would have caused our line of sight to the central object to cross different regions of the system near phase zero in subsequent years. From our observations it appears that during the years 1984 to 1986 we get a progressively better view of the central source: i.e., an obscured view during 1984, and a much clearer view during the 1986 observations. This might for example be caused by a "hot spot" (a thickening of the outer disk at the point where the stream from the secondary impacts it), being in the line of sight during the 1984 observation but having rotated away during the later observations. Alternatively, the stream itself could play a role in obscuring the central source.

Varying obscuration of the flux from the source may also resolve the problem of super-Eddington fluxes in Cir X-1(i.e. the observed persistent flux is sometimes higher than the flux as observed during a radius-expansion burst, which is expected to be very close to the Eddington limit). The flux we have seen during the radius expansion burst of Cir X-1 (which occurred in observation F; Tennant et al., 1986b; see also Stewart et al. 1991), may have been partly obscured. At other phases less obscuration may take place and the flux can seem to be super-Eddington (Stewart et al. 1991).

We note that a *precessing* accretion disk might produce a qualitatively similar set of (obscuration) effects that gradually varies through the years. Our present analysis can not distinguish between these two options. The ratio of the long-term period (possibly a precession period) to the orbital period is in other systems in the range ~12–50 (Priedhorsky & Holt 1987), so the precession period in Cir X-1 could be a few years.

The apsidal motion hypothesis as well as the precessing disk hypothesis predict that changes in phase zero behaviour are *periodic* with a period of years. We attempted to compare phase zero characteristics observed with other instruments to the EXOSAT observations. However, due to the relatively sparse data coverage, the results of this are inconclusive.

5.3. Comparison with other sources

We now compare the properties of Cir X-1 with those of Z and atoll sources, and black hole candidates (BHCs). The properties of these source types were summarized in Sect. 1.2. For the purpose of our comparison we must keep in mind that obscuration effects due to, for example, the outer disk or stream probably play an important role in the near-phase-zero observations, and that at the mid-phase observations mass transfer to the disk may have ceased and we are witnessing the "emptying-out" of the disk.

Cir X-1 spans a large range in intensity and colours. This range is much larger than usually seen in persistent low magnetic field neutron stars (Z and atoll sources) and in e.g. the persistent BHC Cyg X-1. In Cir X-1 the intensity changes by a factor ~1000, and the colours by a factor ~7, whereas Z sources, persistent atoll sources, and the persistent BHCs and Cyg X-1 and LMC X-3 vary by factors of $\lesssim$5 in intensity and $\lesssim$5 in colours (Balucinska & Hasinger 1991, HK89S). However, the changes of Cir X-1 are similar to those seen in BHC and neutron star *transients* (e.g. Miyamoto et al. 1991). This suggests that large changes in $\dot{M}$ underlie these large variations.

5.3.1. Comparison with atoll sources

In the phase zero low state (<1 c/s/cm^2) data we see that the power spectra have a power-law shape with a similar slope as atoll sources in the banana state. The rms increases with flux, which is also similar to what is seen in atoll sources. However,

the measured rms amplitudes in Cir X-1, ~5-35%, are in general higher than those obtained for atoll sources (typically 1-5%, see HK89). As already noted, also the motion in CD and HIDs has a much larger amplitude in Cir X-1 than in atoll sources.

Mid-phase observation G, on the other hand, shows behaviour that is very similar to that of an atoll source in the banana state. A small curved branch is visible in CD and HIDs, and the power spectrum has a *very low frequency noise* component with an rms amplitude of 2.4% to 4.2% increasing from the lower banana to the upper banana. The change in the rms amplitude of the *high frequency noise* component is consistent with either a decrease from lower to upper banana or with no change. This behaviour is also found in atoll sources (HK89): the VLFN rms amplitude increases from the lower to the upper banana, while the HFN component decreases from the lower to the upper banana. Typical power law indices found in atoll sources in this state are ~1.1–1.4, while in Cir X-1 it ranges from 1.8–1.9. The values which are found for the cut-off frequency of the *high frequency noise* component are somewhat smaller than usually found in atoll sources (2–6 Hz vs. 12–25 Hz). However, 4U 1608-52 and 4U 1705-44 show a different behaviour (Yoshida et al. 1993; Langmeier et al. 1989)

Atoll sources in the island state show (sometimes quite strong) band limited noise and then become similar to BHCs in the low state (see e.g. van der Klis 1994b). We will discuss the Cir X-1 observations showing strong band limited noise in the section where we compare the source with the BHCs.

5.3.2. Comparison with Z sources

During observation H after the intensity step, Cir X-1 shows a pattern in the CD and HIDs which consists of a one-dimensional track with sharp bends that divide the track into "branches". This is reminiscent of the CD behaviour of Z sources. However, the orientation of the branches in the CD is different from that in Z sources. Among Z sources differences in branch orientation in the CD and HIDs between sources as well as between different observations of one source occur (Hasinger 1988; Kuulkers et al. 1994c; Kuulkers & van der Klis 1994), but the CD track of Cir X-1 does not fit into the range of those observed in Z sources.

The 6–20 Hz QPO observed when the source flux is highest, on the other hand, is very reminiscent of the normal and flaring branch QPO in Z sources. In Z sources, normal branch QPO (NBO) are found in a portion of the normal branch with a frequency near 6 Hz. Flaring branch QPO (FBO) are found with a frequency which increases from ~6 to ~20 Hz. Both NBO and FBO have a low harmonic content: no harmonics have been detected. Between the NB and the FB there is a sharp bend in the CD track. NBO/FBO occur when $\dot{M}$ is highest, probably near the Eddington critical rate (whether the X-ray intensity is highest at that instant appears to depend on source inclination, Kuulkers et al. 1994a) and there is a positive correlation between frequency and mass accretion rate. The QPO observed in Cir X-1 in observation H resemble this pattern very much: at the highest fluxes QPO with a frequency of ~20 Hz are found. This frequency decreases to ~6 Hz when the flux decreases and there is a sharp bend in the track in the CD when the frequency reaches 6 Hz. The QPO show no harmonics. The flux during observation H is high and the source is probably close to the Eddington luminosity, as the flux is comparable to that of the first type I burst in observation F, which shows radius expansion (Tennant et al. 1986b). The peak flux during observation H is ~ 2 times the peak flux of the burst.

5.3.3. Comparison with black-hole candidates

When the source is bright to very bright the power spectra of Cir X-1 *also* have considerable similarities with those found in black-hole candidates. In observation D, during the big flare, the power spectrum is reminiscent of that of Cyg X-1 in the low state: it is flat below ~0.01 Hz, and the total power is very high (~40% rms). During observation H after the step the power spectrum of Cir X-1 is similar to that of BHC spectra in the very high state, except that the frequencies of the QPO are 6–20 Hz and have a low harmonic content (like in Z sources in the NB/FB) rather than 2–10 Hz with strong harmonics (as is seen in BHCs). The spectrum shows band limited noise with a cut-off frequency of 3-30 Hz and a fractional rms variation of 3–7%. The band limited noise shape changes seen in BHCs are also present in Cir X-1, but they take place on a longer time scale (10^3 s) than in BHCs (1 s). The CD/HID branches in Cir X-1 in this state are also similar to those seen in BHCs in the very high state, in that they seem to be less repeatable than in Z sources.

5.3.4. Interpretation of atoll/Z/BHC similarities

We now interpret the results of our comparison of the CD/HID and power spectral properties of Cir X-1 to those of other accreting compact objects in terms of the variable obscuration/accretion scenario described in Sect. 5.1.

The *phase zero low-flux states* (<1 c/s/cm^2) all show power law noise that is much stronger than the power law noise seen in Z and atoll sources, and in BHCs in the high state. We conclude that it is unlikely that this power law noise in Cir X-1 is similar to that in other sources. As these phase zero low states are probably due to obscuration, it seems likely that inhomogeneities in the obscuring medium are responsible for the fluctuations that produce these power spectra.

The *mid-phase observations* in our interpretation show the source in a state where mass transfer to the disk has ceased and we witness the process of a disk emptying itself out onto the neutron star. In observation C we see peculiar flares which are unlike any other type of variability seen in accreting compact objects. We interpret this as the consquence of an instability that occurs in a low-density, nearly depleted disk. In observation E we see very little flux; the disk may have nearly depleted itself here. The X-ray spectrum in this observation is the hardest we have observed in Cir X-1. This is in accordance with other findings that at low $\dot{M}$, X-ray spectra become very hard (Van Paradijs & Van der Klis 1994). That the X-ray spectrum of the *phase zero* observations at similarly low count rates does

not become hard is additional evidence that the phase zero low states are not due to a low $\dot{M}$, but to obscuration. In observation G, finally, we see behaviour that is very similar to that of an atoll source in the banana state, which makes it attractive to hypothesize that here the disk is still in a more or less normal (non-depleted) state and Cir X-1 is really behaving like an atoll source at this time.

Of the *phase zero bright states*, first consider the post-step part of observation H. During this time, the band limited noise and the morphology of the branches resemble those seen in a BHC in the very high state, whereas the QPO resemble that of a Z source in the normal or flaring branch. We interpret the behaviour at this time as due to near-Eddington accretion onto a neutron star with a magnetic field strength that is lower than that in Z sources (see also van der Klis 1994c). The BHC-like properties of Cir X-1 in this observation are then due to the absence, like in BHCs but unlike in Z sources, of a magnetic field that is strong enough to affect the observable properties of the accretion flow. The Z-source-like properties which are observed simultaneously are due to the presence of a neutron star rather than a black hole in the system. The unique combination of these two sets of characteristics is interpreted as due to the fact that Cir X-1 is the *only* known neutron star with a magnetic field as low as in atoll sources (i.e., too low to cause observable effects) that sometimes reaches Eddington accretion rates. The source is therefore of great importance, as it allows to separate out phenomena that are related to the black-hole character of the compact object from those that are related to "just" the weakness of its magnetic field. We conclude that frequency and harmonic content of the near-Eddington QPO are apparently directly related to compact object type (neutron star or black hole), with the presence of strong harmonics a possible black hole signature, and the 6-Hz lower bound to the frequency range of the QPO a neutron star signature. We further conclude that the strong band limited noise with variable shape is apparently a consequence of near-Eddington accretion onto low magnetic field compact objects (either neutron stars or black holes) and is in some way suppressed by the magnetic field of Z sources.

Now consider the big flare near phase zero in observation D. During this flare, the power spectrum of Cir X-1 resembles that of a BHC in the low state. In accordance with what has previously been seen in the atoll sources 4U 1608-52 and 4U 1705-44 (Yoshida et al. 1993; Langmeier et al. 1989), this shows that a low magnetic field neutron star can sometimes appear like a BHC in the low state, with strong (several 10%) band limited noise with a low (roughly 0.01 Hz) cut-off frequency. There is an apparent contradiction in the relatively high count rate of Cir X-1 (1.2 c/s/ cm^2) during this "BHC low state-like" episode as compared to the 0.6 c/s/cm^2 count rate in observation G, when no obscuration should occur as it was at mid-phase, and when the source was in an "atoll banana-like" state, which is similar to a BHC high state (van der Klis 1994b, see Sect. 1.2). We note that a similar paradox exists in BHCs: there also, in some cases, particularly in the transient GS 2023+338, low state-like behaviour is observed at relatively high luminosity (Miyamoto et al. 1992). Two possible solutions have been proposed for this. One is that there exists an additional state that at high L_x mimicks the BHC low state (Nowak 1994). The other is that the *viewing geometry* determines at what L_x level the transition between low state and high state occurs (van der Klis 1994c). In this interpretation low state behaviour occurs when we can see the central part of the accretion flow. When $\dot{M}$ increases the inner, radiation pressure dominated part of the disk thickens and hides the central region from our view, thus ending the low state. When, for example due to a low inclination we can look down a polar funnel of the thickening accretion disk up to higher $\dot{M}$ levels, then the low state extends to higher L_x levels. In the case of Cir X-1, this would mean that between observation D and observation G a change in viewing geometry must have occurred allowing us to look down to the central engine up to higher accretion rate levels in observation D than in observation G. This change might be related to the apsidal motion or disk precession discussed in Sect. 5.1. To test this, further observations are required to look for possible long-term periodicities in the phenomenology of Cir X-1, which could confirm that apsidal motion or disk precession are taking place in the system.

6. Summary

We have interpreted the complex properties of Cir X-1 in terms of a model of an accreting neutron star with a magnetic field strength that is too low to have observable effects on the accretion flow (an atoll source). What in our interpretation makes the source unique is its location in a highly eccentric 17-d binary, causing near-Eddington mass accretion to occur near periastron. This has two consequences: (i) it causes obscuration effects related to the sudden onset of rapid mass transfer, which leads to phenomena that may be unique to Cir X-1, such as power law noise with amplitudes up to 35% (rms) and very sudden very large intensity transitions (we note that such phenomena might also be observable during the *onset* of transient accretion events in soft X-ray transients), and (ii) it produces near-Eddington accretion rates onto an atoll source, which does not otherwise occur. This produces behaviour that has elements of neutron star characteristics (particularly, 6–20 Hz QPO with a low harmonic content) as well as those of BHC (particularly, strong and variable band limited noise). This makes Cir X-1 very important for our understanding of the similarities in the observable properties of accreting neutron stars and accreting black holes, as it allows to separate out the properties that are unique to BHCs from those that are merely unique to accreting compact objects with a low magnetic field.

We have concluded that in addition to a mass transfer rate that is highly variable with binary phase another ingredient is likely required in order to explain Cir X-1's phenomenology, and that this additional ingredient probably is one that causes changes in the viewing geometry on time scales >1 yr. Apsidal motion and disk precession are candidates for this additional ingredient; further observations are required to see whether the periodicity in viewing geometry predicted by both mechanisms does indeed occur.

Acknowledgements. This paper was supported in part by the Netherlands Organization for Scientific Research (NWO) under grant PGS 78-277. WHGL is supported by the United States National Aeronautics and Space Administration under grant NAG8-700. JVP acknowledges NATO RG 88/033.

References

Andrews, D., Stella, L., 1985 EXOSAT Express 10, 35
Balucinska, M., Hasinger G., 1991, A&A 241, 439
Belloni, T., Hasinger, G., 1990, A&A 227, L33
Berger, M., van der Klis, M., 1994, A&A 292, 175
Dieters, S., van der Klis, M. 1995, in preparation
Hasinger, G., van der Klis, M., 1989, A&A 225, 79 (HK89)
Inoue, H., 1992 ISAS RN 518, to appear in Accretion disks in compact Stellar Systems, J.C. Wheeler (ed.).
Jones, C., Giaconni, R., Forman, W., Tananbaum, H., 1974, ApJ 191 L71
Kahn, S., Grindlay, J.E., 1984, ApJ 281, 826
Kaluzienski, L.J., Holt, S.S., Boldt, E.A., Serlemitsos, P.J., 1976, ApJ 208, L71
Kuulkers, E., van der Klis, M., 1994, in prep.
Kuulkers, E., van der Klis, M., van Paradijs, J., 1995 ApJ submitted
Kuulkers, E., van der Klis, M., Oosterbroek, T., Asai, K., Dotani, T., van Paradijs, J., Lewin, W.H.G., 1994a, A&A 289, 795
Kuulkers, E., van der Klis, M., Oosterbroek, T., van Paradijs, J., Lewin, W.H.G., 1994b, in prep.
Langmeier, A., Hasinger, G., Trümper, J., 1989, ApJ 340, L21
Leahy, D. A., Darbro, W., Elsner, R. F., Weisskopf, M. C., Kahn, S., Sutherlands, P. G., Grindlay, J.E., 1983, ApJ 266, L160
Lewin, W.H.G., Van Paradijs, J., van der Klis, M., 1988,Space Sci. Rev. 46, 273
Lewin, W.H.G., van Paradijs, J., Taam, R.E., 1993 Space Sci. Rev., 62, 223
Makino, Y., Kitamoto, S., Miyamoto S., in Frontiers of X-ray Astronomy, Proc. 23d Yamada meeting, Y. Tanaka & K. Koyama (eds.), Universal Academy Press, Tokyo, p. 167
Margon, B., Lampton, M., Bowyer, S., Cruddace, R., 1977 ApJ 169, L23
Miyamoto, S., et al., 1991 ApJ, 383, 784
Miyamoto, S., et al. 1992, in Proc. Ginga Memorial Symposium, F. Makino & F. Nagase (eds.), ISAS, Tokyo, p. 37
Miyamoto, S., et al., 1993, ApJ 403, L39
Moneti, A., 1992, A&A, 260,L7
Murdin, P., Jauncey, D.L, Haynes, R.F. et al., 1980, A&A 87, 292
Nowak, M.A., 1994, ApJ 422, 688
Nicolson, G.D., 1980, IAU Circ. No. 3449
Priedhorsky, W., Holt, S.S., 1987, SSRv 45, 291
Stewart, R.T., Nelson, G.J., Penninx, W., Kitamoto, S., Miyamoto, S., Nicolson, G.D., 1991, MNRAS 253, 212
Stewart, R.T., Caswell, J.L. Haynes, R.F., Nelson, G.J., 1993, MNRAS 261, 593
Sztajno, M., van Paradijs, J., Lewin, W.H.G., Langmeier, A., Trümper, J., Pietsch, W., 1986 MNRAS 222, 499
Tanaka, Y., Lewin, W.H.G. In: X-ray Binaries, W.H.G. Lewin, J. van Paradijs, E.P.J. van de Heuvel (eds.), Cambridge University Press, 1994, in press
Tennant, A.F., Fabian, A.C., Shafer, R.A., 1986a, MNRAS 219,871
Tennant, A.F., Fabian, A.C., Shafer, R.A., 1986b, MNRAS 221,27p
Tennant, A.F., 1987, MNRAS 226, 971
Tennant, A.F., 1988a, MNRAS 230, 403
Tennant, A.F., 1988b, Adv. Space Res. 8, 397
Toor, A., 1977, ApJ 215, L57
Turner, M. J. L., Smith, A., Zimmerman, H.U., 1981, Sp. Sci. Rev. 30, 513
Van der Klis, M., 1989a, ARAA 27, 517
Van der Klis, M., 1989b, in: Timing Neutron Stars, H., Ögelman, E.P.J. van den Heuvel (eds.), Kluwer Academic Publishers, p. 27
Van der Klis, M., 1991, in: Neutron Stars: Observations and Theory, J. Ventura, D. Pines (eds.), Kluwer Academic Publishers, p. 319
Van der Klis, M., 1994a in: Lives of the neutron stars, M.A. Alpar and J. van Paradijs (eds.), Kluwer Academic Publishers.
Van der Klis, M., 1994b, A&A 283, 469
Van der Klis, M., 1994c, ApJSupp 92, 511
Van der Klis, M., Lamb, F.K., 1994, ARAA in preparation
Van Paradijs, J., Van der Klis, M., 1994, 281, L17
Penninx, W., Lewin, W.H.G., Mitsuda, K., van der Klis, M., van Paradijs, J., Zijlstra, A.A, 1990, MNRAS 243, 114
White, N.E., Peacock, A., 1988, Mem. S. A. It. 59, 7
Yoshida, K., Mitsuda, K., Ebisawa, K. et al., 1993, PASJ 45, 605

This article was processed by the author using Springer-Verlag LaTeX A&A style file version 3.